Geoderma 438 (2023) 116625

Contents lists available at ScienceDirect

Geoderma

journal homepage: www.elsevier.com/locate/geoderma

Microscale spatiotemporal patterns of water, soil organic carbon, and enzymes in plant litter detritusphere

Kyungmin Kim [a,b,c,*], Anders Kaestner [d], Maik Lucas [a,b], Alexandra N. Kravchenko [a,b]

[a] Department of Plant Soil and Microbial Sciences, Michigan State University, MI, USA
[b] DOE Great Lakes Bioenergy Research Center, Michigan State University, MI, USA
[c] School of Integrative Plant Science, Cornell University, NY, USA
[d] Paul Scherrer Institut, Villigen, Switzerland

ARTICLE INFO

Handling Editor: A. Agnelli

Keywords:
Decomposition
Zymography
Enzyme
Microbial Hotspots
Soil Carbon
Neutron Tomography

ABSTRACT

Understanding biophysical and biochemical processes in detritusphere is critical to quantifying and modeling plant residue decomposition dynamics and subsequent soil organic carbon (C) accrual. The objectives of the study were to explore (i) micro-environmental conditions within the detritusphere formed around decomposing corn and soybean leaves, and (ii) the relationships between moisture distribution, enzyme activity, and C dynamics during decomposition. We assessed spatial and temporal dynamics of moisture distribution using X-ray and neutron computed tomography, and activities of β-glucosidase and chitinase, two enzymes involved in soil C and N processing, using zymography. We used ^{13}C labeled residue to track residue contribution to atmospheric CO_2 and soil organic C. Moisture redistribution pattern varied depending on the residue type. While the water was immediately absorbed by the corn leaves and maintained afterward, switchgrass leaves absorbed water more slowly and created water-deficient zones within ~1mm from the residue. This initial moisture depletion led to lower chitinase activity and residue-derived CO_2 emissions in switchgrass. In contrast to chitinase, β-glucosidase activity was influenced by a combination of vegetation history and residue type, and it was higher when the origin of the residue matched the vegetation history of the soil. Pore size had an opposite impact on the studied enzymes, supporting the notion that contrasting soil pore architecture can stimulate activities of different enzymes through a selection of dominant enzyme producers. We concluded that the decomposition dynamics of plant residues is not only a simple function of residue chemistry, but rather a combined effect of the vegetation history, in part through its effect on microbial community composition, the plant residue chemical and likely physical characteristics, and the soil pore structure in the detritusphere. Together, they create temporally dynamic micro-environmental conditions influencing decomposition. Specifically, our study demonstrated that the initial micro-environment formulated in detritusphere can play an important role in enzyme activities and consequent C dynamics.

1. Introduction

Soil organic carbon (SOC) sequestration is one of the important keys to mitigate atmospheric CO_2 levels as emphasized in the 'Soil carbon 4 per mille' initiative (Minasny et al., 2017). Plant residue incorporation is a management strategy that can maximize new C inputs, and thus can be a valuable pathway to increase SOC (Liu et al., 2014). During decomposition of incorporated residue, some of the resultant products can be stabilized within the soil matrix increasing SOC stocks (Jiang et al., 2017; Cotrufo et al., 2019; Hunt et al., 2020; Georgiou et al., 2022), yet others might stimulate greenhouse gas emissions (CO_2 and N_2O) (Thangarajan et al., 2013; Köbke et al., 2018; Kim et al., 2020) and induce positive priming (Kuzyakov et al., 2000; Kuzyakov, 2010; Shahbaz et al., 2017a). Properties of organic substrates (i.e., residues) added to the soil (Shahbaz et al., 2018), composition of microbial communities which utilize the substrates (Arcand et al., 2016), and physical characteristics of micro-habitats populated by the microbial communities (Toosi et al., 2017) together determine the rates and pathways of microbial processes involved in residue decomposition (Seyfried et al., 2021).

A plant residue fragment creates a unique environment within the soil in its immediate surrounding, a.k.a. detritusphere (Liu et al., 2011).

* Corresponding author at: School of Integrative Plant Science, Cornell University, Ithaca, NY, USA.
E-mail address: kk785@cornell.edu (K. Kim).

https://doi.org/10.1016/j.geoderma.2023.116625
Received 21 October 2022; Received in revised form 26 March 2023; Accepted 29 July 2023
Available online 3 August 2023

Detritusphere differs from the bulk soil (that is, the soil not affected by the residue presence), by its distinct microbial community composition (Poll et al., 2006; Poll et al., 2008), higher microbial biomass (Marschner et al., 2012; Hoang et al., 2016), enzyme activity (Poll et al., 2006) and nutrient concentrations (Gaillard et al., 1999; Gaillard et al., 2003; Vedere et al., 2020). Decomposing residues also create micro-scale gradients of soil moisture in their immediate vicinity (Kim et al., 2020) due to moisture absorption by the residue, a.k.a. sponge effect (Kravchenko et al., 2017; Kutlu et al., 2018; Kravchenko et al., 2018). The soil moisture gradients can further affect microscale distribution patterns and persistence of SOC (Schlüter et al., 2022).

Activity of extracellular enzymes within the soil can be used as an indicator of microbial involvement in decomposition of both fresh organic substrates (Sinsabaugh and Moorhead, 1994; Allison and Vitousek, 2004) and native soil organic matter (Shahbaz et al., 2017b). Recent developments in 2D zymography, a non-destructive technique to measure *in situ* activity of hydrolytic enzymes (Sphon and Kuzyakov, 2013; Razavi et al., 2019; Sanaullah et al., 2016; Guber et al., 2021) enable testing the links between enzyme activities and C gains/losses. Two hydrolytic enzymes of particular interest are β-1,4-glucosidase and β-*N*-acetyl-glucosaminidase (chitinase), since they are utilized at different stages of residue decomposition, e.g., degradation of cellobiose and chitin (Sinsabaugh et al., 2008). With zymography, the same soil surface can be repeatedly used for 2-dimensional enzyme mapping, enabling quantification of the temporal dynamics of enzyme activity at specific locations.

The strength of enzyme activity within the detritusphere is affected by the chemical characteristics of the plant residue. Plant residues with low C:N ratios and high labile C often elicit stronger enzyme activities, thus faster residue decomposition, as compared to the residues with high C:N ratios and low labile C (Veres et al., 2015; Stewart et al., 2016). The intrinsic differences in microbial biomass and community composition also affect enzyme activity. E.g., soils under perennial vegetation often have more diverse microbial communities and higher microbial biomass than annual cropping systems, with concomitantly higher enzyme activity (Culman et al., 2010; Cattaneo et al., 2014; McGowan et al., 2019; Kasanke et al., 2021). Micro-environmental conditions in detritusphere can also influence the enzyme activity – including both enzyme production and subsequent effectiveness of the produced enzymes (Burns et al., 2013). For instance, surface characteristics of the plant residues (Allison and Vitousek, 2004) and soil pore architecture (Poll et al., 2006; Burns et al., 2013) can alter the transport of enzymes and substrates thus affecting decomposition rates and microbial access to degradation products. Greater water availability in the vicinity of decomposing residues, aka sponge effect (Iqbal et al., 2013; Kravchenko et al., 2017; Kim et al., 2020; Li et al., 2022), can facilitate the enzyme production and activity (Geisseler et al., 2011). Yet, the combined influences of the sponge effect, residue type, and vegetation/management history on activities of soil enzymes have not yet been thoroughly investigated.

Quantification of the temporal dynamic in distribution of water inside the decomposing residues and in their vicinity is crucial for understanding micro-environmental conditions during residue decomposition. Recently, the water distribution within and around the decomposing residue was assessed via dual-energy X-ray computed tomography (xCT) scanning with potassium iodide solution as a dopant (Kim et al., 2020), an approach that assumes that the spatial distribution of iodine (I^-) is represnetative of the water distribution with the soil pores. However, a possibility of preferential absorption of I^- by organic materials (Yamaguchi et al., 2010), including residues, raises a concern that this approach might overestimate the extent of the sponge effect. Neutron computed tomography (nCT) allows direct detection of water (Lehmann et al., 2006) due to strong absorbance of neutrons by hydrogen containing compounds and its relatively weak interactions with other materials (Moradi et al., 2011; Tötzke et al., 2017). Recent development of time series nCT allowed to quantify the hydraulic redistribution in the plant root system (Hayat et al., 2020; Tötzke et al., 2017; Zarebanadkouki et al., 2015). The same technique can be used for tracking water redistribution near plant residues decomposing within the soil.

The objectives of this study are (i) to assess spatial and temporal dynamics of moisture distribution and enzyme activity in vicinity of plant residues decomposing within the soil, and (ii) to explore relationships between moisture distribution, enzyme activity, and C dynamics during residue decomposition. We investigated spatial and temporal trends in water, enzymes, and residue-derived C distributions during decomposition of leaves of ^{13}C-labeled corn (*Zea mays* L.) and switchgrass (*Panicum virgatum* L.), the two plant species with contrasting C:N ratios, incorporated into soils of contrasting vegetation history and pore size characteristics.

2. Materials and methods

2.1. Soil and plant residue preparation

Soils used for the experiment were collected from Long-Term Ecological Research (LTER) site at W. K. Kellogg Biological Station (KBS), Michigan, U.S.A. The soil is Kalamazoo loam (fine loamy, mixed, mesic, Typic Hapludalf), developed on glacial outwash and containing 43% sand and 17% clay (Robertson and Hamilton, 2015) with 0.9% of total C and 0.1% of total N concentrations (Grandy and Robertson, 2007). The two studied contrasting vegetation histories were the annual cropping system, i.e., conventionally managed and plowed corn-soybean-wheat rotation (CSW) and the perennial grassland vegetation, i.e., monoculture switchgrass (SG), established in 2008.

Soil for the experiment was collected in Fall 2020 from 5 to 15 cm depth, air-dried, cleaned from visible plant residue and root fragments, and used to create soil materials with contrasting pore size characteristics, namely: (i) the large pore material with dominance of >30 μm Ø pores, and (ii) the small pore material with dominance of <10 μm Ø pores. The materials were created from CSW and SG soils following the procedure described in Toosi et al. (2017). In brief, a large pore material consisted of 1–2 mm soil aggregate fraction and was obtained by sieving the soils through 1 mm and 2 mm mesh. In additions, a small pore material was obtained from the large pore material by gently pushing it through 0.053 μm mesh. The remaining stones and large mineral grains were ground using a shatter box until also passing the 0.053 μm mesh. This approach allowed us to minimize microbial and mineralogical differences between the two materials (Kim et al., 2020). X-ray computed tomography analyses of these materials verified that their pore size distributions differed, with >30 μm and <10 μm Ø pores indeed prevailing in the large and small pore materials, respectively (Toosi et al., 2017).

In order to obtain ^{13}C labeled plant residues, corn and switchgrass were grown in controlled greenhouse settings and labeled with ^{13}C as described in Kim et al. (2022). After the labeling, the leaves for this experiment were harvested, washed with distilled water, and dried in a botanical press for 4 weeks. The labeled corn and switchgrass leaves used in the study had δ^{13}C signatures of 864 and 822 ‰, respectively.

2.2. X-ray and neutron tomography

To explore water distribution within and around corn and switchgrass leaf residues, xCT and nCT of soil samples with incorporated leaves were performed using the cold neutron imaging beamline ICON at Paul Scherrer Institut (PSI), Villigen, Switzerland (Kaestner et al., 2011; Kaestner et al., 2017). Due to time and labor consuming nature of nCT analyses and a very limited beamtime available for the experiment, only a few of the studied treatment combinations could be subjected to joint xCT and nCT. We prioritized the comparison between the residues of the two plant species, and, thus, used only the large pore soil material for these analyses. Based on our past results (Kravchenko et al., 2017; Kim et al., 2020) we expected that the influence of plant residue on water

distribution will be the greatest when pore architecture is dominated by large pores. We also did not expect that the soil vegetation history will substantially influence the short-term water distribution patterns that we aimed at assessing using nCT in this study. Thus, a 1:1 mixture of large pore materials of CSW and SG soils was used. One soil sample was prepared for each plant species, where 3 leaf circles per sample provided a measure of variability among the individual plant residue fragments and their immediate surroundings (Fig. 1).

To prepare the samples, metal columns with 8 mm Ø and 20 mm height were filled with the large pore soil material. Three disks (6 mm Ø) cut from press-dried corn and switchgrass leaves were embedded into each column, separated by ~4.5 mm soil layers. Each column contained 1 g of soil packed to 1.35 g/cm^3 density. First, the columns were subjected to xCT scanning in an air-dry state. Then, 1 mL of H_2O was added on the top of each column followed by time series nCT scanning. The nCT scanning was conducted by uniform stepping method for a duration of 19 h by 1 h step. Detailed tomographic settings were provided in Supplementary material (S1. Neutron Scanning).

Since the xCT and nCT scans differed in their scanning window and resolution parameters, the images were registered using BigWarp Plugin in Fiji (Bogovic et al., 2016; Schindelin et al., 2012). The detailed procedure is provided in the Supplementary Material (S2. Image registration). After image alignment, pore-solid segmentations were conducted, and locations of leaf disks were identified from the xCT images (provided in S3. Leaf detection). Then the leaf image masks were overlayed with nCT images, and grayscale values from nCT images were obtained for a range of distances from each leaf in the soil column using Euclidean distance map in Fiji (at a 1-voxel distance step). When a pixel was classified as a pore, the grayscale value of that pixel was labeled 'NaN' and not included in calculations. In order to ensure comparability between the soil columns and the images obtained from the same column at different scanning times, the grayscale values at each distance were normalized by dividing them by the mean grayscale value of the whole soil column. The normalized grayscale value (normGV) of the entire soil column was thus equal to 1. The normGVs were used as a proxy of moisture contents due to high attenuation of hydrogen to neutrons (Tengattini et al., 2021).

2.3. Water absorption by plant leaves

Water absorption by corn and switchgrass leaves incorporated into the soil was also directly assessed in a separate experiment. For the experiment, corn and switchgrass leaves were allowed to absorb water within soil cylinders filled with either large or small pore materials. The cylinders were prepared as described by Kim et al. (2021) with three replicated cylinders used for every soil material and plant combination. Specifically, each cylinder (30 mm Ø x 60 mm h) consisted of 5–6 plant leaf disks of the known mass (6.6–13.9 mg) placed in between two 30 mm layers of the soil materials. The materials were first packed to 1.3 g/cm^3 bulk density. Then water was added to the cylinders with a spray bottle to adjust the soil moisture content to 50% water-filled pore space (WFPS). After 4 h, the cylinders were disassembled, and the plant leaf disks were cleaned of attached soil using a small brush and weighed. The quantity of water absorbed by the residue from the surrounding soil was then determined from the difference between the initial and final leaf weights.

2.4. Incubation experiment

Plant residue decomposition and its effect on surrounding detritusphere were studied using soil microcosms. The microcosms were built within transparent plastic containers, 4.7 cm x 2 cm x 3.3 cm (width x height x depth) in size with removable front panels. Each microcosm contained 30 g of soil and 30 mg of plant residue (or 0 mg in case of control samples). The residue was placed horizontally in the middle of the container (Fig. 2A). To build a microcosm, 15 g of soil was packed to ~ 1.1 g·cm^{-3} bulk density and soil moisture was adjusted to 50% WFPS. After that, the plant residue was placed in a single flat layer on the

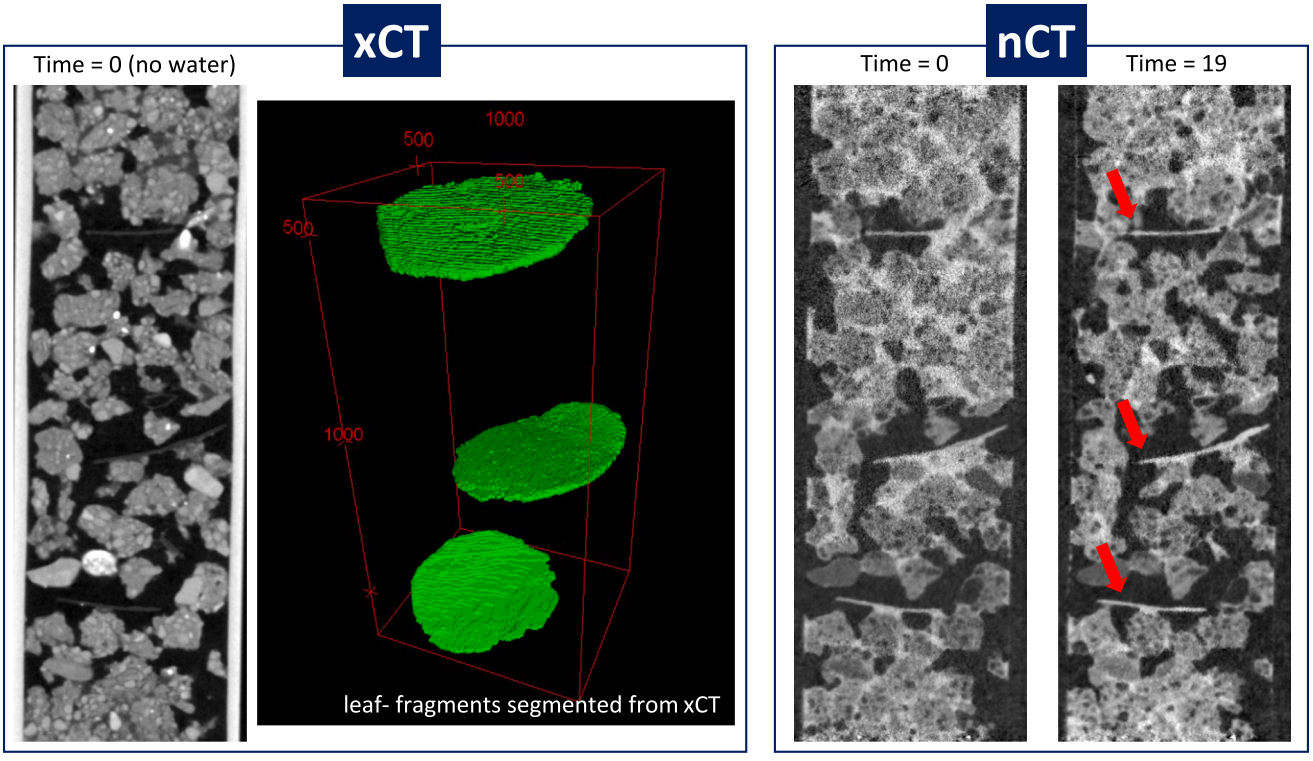

Fig. 1. Sample xCT (left) and nCT (right) images of a scanned microcosm (large pore dominated soil), along with images of the leaves (green disks) incorporated within the sample and identified using xCT (center). Column diameter is 8 mm. After water addition, the same samples were subjected to nCT every 1 h, for 19 h, images from t=0 and t=19 are shown. Red arrows point to the leaf fragments visible on nCT images.

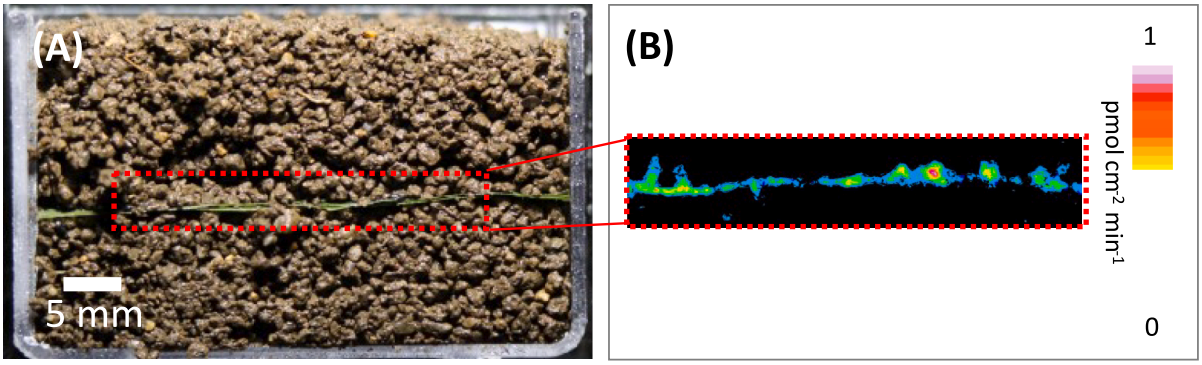

Fig. 2. Schematic representation of zymography procedure. (A) Plant leaf embedded within soil microcosms used for zymography. A box with red dotted line shows the location where a polyamide membrane saturated with fluorogenic substrate was attached. (B) The example enzyme activities in close proximity to the leaves (the same red dotted box with (A)).

surface of the soil using forceps. Another 15 g of the soil was added on top of the residue layer and water was added to achieve 50% WFPS. Water was added using a 20 mL spray bottle so as not to disturb soil arrangement. A total of 52 microcosms were created, consisting of 5 replications of all combinations of the two soil vegetation histories (CSW and SG), two pore size materials (large and small pore materials), and two residue types (corn and switchgrass) (a total of 40) and of control samples with 3 replicates for each combination of vegetation history and pore size (a total of 12).

Each soil microcosm was placed within a 450 mL Mason jar containing a small beaker with 8 mL of distilled water to minimize moisture losses from the microcosms. Mason jars were sealed tightly and kept in the dark at 20 °C for the 22 days of the incubation experiment. During the incubation, CO_2 and $^{13}CO_2$ in the headspace and the enzyme activity were measured on days 1, 3, 8, 15, and 22. On each day, the headspace gas was sampled using a syringe and injected into 5.9 mL storage vials (Labco Ltd, Lampeter, U.K.) at 2 atm pressure. Two replicate microcosms from each combination of treatment were subjected to β-glucosidase zymography and other 2 replicates were subjected to chitinase zymography. Zymography measurements were performed after gas sampling, and the microcosms were placed back into the Mason jars after zymography until the next gas measurement. Jars were flushed using ambient air and sealed before returning to the incubation chamber. Due to an operational error, chitinase measurements on day 1 were not completed. After the incubation, i.e., on day 22, soil microcosms were dissected into eight 4-mm-thick layers parallel to the plant residue using thin blades. Individual layers were air-dried for 2 days, homogenized, and subjected to soil organic C (SOC) and ^{13}C analysis.

CO_2 concentration of the sample headspace gas was analyzed using LI-COR infrared gas analyzer. SOC was analyzed using Costech elemental combustion system (Costech Analytical Technologies Inc., CA, U.S.A). Isotopic composition of CO_2 was measured using an IsoPrime 100 stable isotope ratio mass spectrometer (IRMS) interfaced to a Tracegas inlet system (Elementar, Mt. Laurel, NJ). $\delta^{13}C$ in solid samples, i.e., soil and KCl extract powder, were performed using an Isoprime Vision IRMS interfaced to a Vario Isotope Cube elemental analyzer (Elementar).

2.5. Assessment of plant-derived C

Relative differences in isotopes to the standards (δ) were obtained from the isotopic analysis and converted to atomic percent (Atom%) to calculate plant-derived C in CO_2 and SOC:

$$Atom\%^{13}C = \{[(\delta \cdot 1000^{-1} + 1) \cdot {}^{13}C/{}^{12}C]^{-1} + 1\}^{-1} \cdot 100 \quad \text{Eq. (1)}$$

Fraction of plant-derived carbon fC_{plant} was calculated as:

$$fC_{plant} = (Atom\%\ {}^{13}C_{trt} - Atom\%\ {}^{13}C_{control}) \cdot (Atom\%\ {}^{13}C_{plant} - Atom\%\ {}^{13}C_{control}) \quad \text{Eq. (2)}$$

where $Atom\%^{13}C_{trt}$ is the atom% of ^{13}C in CO_2 gas or SOC of the treatment sample, $Atom\%^{13}C_{control}$ is the atom% of natural ^{13}C abundance in an unamended sample, and $Atom\%^{13}C_{plant}$ is the atom% of ^{13}C in the labeled plant leaves. Then the concentration of the CO_2 or SOC derived from the labeled plant leaves (C_{plant}) was calculated as following:

$$C_{plant} = C_{total} \cdot fC_{plant} \quad \text{Eq. (3)}$$

where C_{total} values were directly obtained from either CO_2 and SOC measurements.

Priming rates were calculated by subtracting soil-derived CO_2 emission rate of the control sample from that of the treatment sample. Cumulative priming effect was calculated as the sum of the products of the priming rates and the time intervals from day 1 to day 22.

2.6. Zymography

Spatial and temporal dynamics of the enzymes on the surface of the leaf and in the surrounding soil was measured using time-lapse zymography (TLZ) (Guber et al., 2019). A polyamide membrane filter (0.45 μm pore size; 100 μm thickness, Tao Yuan, China) was saturated in 6 mM fluorogenic substrates specific to β-glucosidase and chitinase (4-Methylumbelliferyl-β-D-Glucoside and 4-Methylumbelliferyl-N-Acetyl-β-D-Glucosaminide, respectively). For zymography, the front panel of the microcosm was opened, sprayed with DI water, and the polyamide membrane was placed on top of the soil surface (Fig. 2A). The microcosm was placed in the dark room with the camera (Canon EOS Revel T6) and ultraviolet light source (Guber et al., 2021; Kim et al., 2022). The membrane on the soil surface was photographed every minute, for a total of 45 min per sample. The enzyme activity was calculated in each individual pixel of the membrane as a highest time derive of MUF content. Zymograms were taken on days 1, 3, 8, 15, and 22 during the incubation. The area (0.27 cm^2 wide) encompassing the residue (Fig. 2B) was used to quantify the enzyme activity in vicinity of residues.

2.7. Statistical analysis

Data were analyzed using a mixed model approach implemented in PROC MIXED procedure of SAS 9.4 (SAS Institute Inc., NC, U.S.A). Statistical models used in the analyses varied depending on the studied soil variable. Specifically, the model for baseline characteristics of the studied soil materials, i.e., C, N, sand, silt, and clay content and C:N ratio, consisted of fixed effects of vegetation history and pore size, along with their interactions. The model for initial characteristics of plant leaf

residues, i.e., C content, C:N ratio, and $\delta^{13}C$, only included the fixed effect of the residue type. For water absorption, the model consisted of pore size, residue type, and their interaction.

Statistical model for the plant-derived C consisted of vegetation history, pore size, residue type, distance (from the residue), and their interactions as fixed effects and soil microcosm, nested within the vegetation history and pore size, as well as replication batches as random effects. Model estimates in each distance, vegetation history, and residue type were compared with 0 using t-tests. In addition, plant-derived C levels at distances of >4 mm and <4 mm from residues were compared using contrasts.

Models for cumulative emission of total CO_2, plant-derived CO_2, and priming effect included fixed effects of vegetation history, pore size, residue type, and their interactions; and a random effect of replication batches. Model estimates of priming effect in each distance, vegetation history, and residue type were compared with 0 using t-tests.

Statistical models for the fraction of CO_2 originated from the leaf residues, β-glucose activity, and chitinase activity consisted of vegetation history, pore size, residue type, time, and their interactions as fixed effects; and replication batches as a random effect. Time was included as a repeated measure factor, the subject for which was the individual soil microcosms.

For all analyses, the assumptions of normality and homogeneity of variances were tested by checking normal probability plots and conducting Levene's test based on the absolute values of model residuals. The data were natural log-transformed when the normality assumption was violated, and the analysis with heterogeneous variances was conducted when the homogeneity of variances assumption was violated.

3. Results

3.1. Properties of the studied soils and plant residues

As a result of grinding and sieving used to procure contrasting pore characteristics, the small pore soil material had lower sand and higher clay and silt contents than the large pore material ($p < 0.05$, Table 1). CSW soils did not show significant differences in C and N contents between pore sizes, while the small pore material of SG soils had slightly higher C and lower N than the large pore material. Corn and switchgrass leaves had similar C contents, but C:N ratio was higher in switchgrass (Table 2). $\delta^{13}C$ signature was higher in corn than in switchgrass residues ($p < 0.05$, Table 2).

3.2. Water distribution in corn and switchgrass leaf residues

Spatial and temporal patterns of water distribution within and around the leaves differed between corn and switchgrass leaves. A proxy of moisture content, normGV, was the highest in close proximity to corn leaves, gradually decreasing with increasing distance and reaching the mean normGV of the entire column, i.e. the normGV of 1.00, at approximately 0.25 mm distance from the leaf. normGV in close proximity to the switchgrass leaves was relatively low, and within the 0.10 mm distance from the leaves, it dropped below the soil's mean normGV, before slowly increasing and reaching the mean at >1 mm distance from the leaves (Fig 3A). The lowest normGV was found at ~0.12 mm distance from the switchgrass leaves, where the value was 0.85 right after water addition, and then it increased and reached 0.97 after 19 h of water addition (Fig. 3A right). Corn residues had normGVs constantly>0.95, indicating that there was less water depletion in their vicinity compared to switchgrass residues.

We visualized the temporal trends at three specific spatial locations: within the leaves themselves (0 mm from the leaves), in close proximity to the leaves (0.1 mm), and at 1 mm distance from the leaves (Fig. 3B). In corn leaves, the normGV increased almost immediately after the start of the incubation. It increased to 1.06 by 3–4 h after the start of the incubation and then remained at that level for the rest of the incubation. On the contrary, switchgrass leaves had normGV of ~0.92 immediately after the water addition. The normGV of the switchgrass leaves then increased reaching 1.00 within ~4 h and continued to grow, albeit slowly, for the rest of the incubation time to normGV of 1.04 at 19 h (Fig. 3B). Approximately 4 h after the water addition, normGVs in both corn and switchgrass leaves reached their respective plateaus (Fig. 3B).

The most drastic difference between the microcosms with corn and switchgrass leaves was observed in close proximity to the leaves (0.1 mm) (Fig. 3B). While normGV in vicinity of corn leaves initially was equal to 1.10 greatly exceeding the average, it then linearly decreased approaching normGV of 1.00 by 19 h of incubation. On the contrary, normGV in vicinity of switchgrass leaves initially was markedly below the average (~0.85), and then increased plateauing at normGV of ~1.00 by 10 h of incubation. At ~1.0 mm from the residues, normGV of both corn and switchgrass microcosms was similar to the average (0.97–1.00) and remained stable during the incubation (Fig 3B).

Direct measurement of moisture contents in the incubated leaves during water absorption experiment were consistent with nCT results (Fig. 3B 0 mm): the corn leaves incubated within the large pore material retained more moisture than the switchgrass ones (Fig 3C). The water absorption results showed that in the small pore materials the corn leaves also absorbed greater amounts of water than the switchgrass leaves.

3.3. Plant-derived C after decomposition

After the 22-day incubation, plant-derived C, measured in the 4-mm thin sections parallel to the leaf surfaces, mostly remained in close proximity of the decomposing residues (Fig. 4 and Table S1). Plant-derived C content was significantly higher at < 4 mm distance from the plant leaves when compared to that at > 4 mm distances ($p < 0.01$). For both soils (i.e., CSW and SG) in the large and small pore soil materials, there was more corn-derived C than switchgrass-derived C within the 4 mm distance from the residue ($p < 0.01$). Soil under conventional agriculture (CSW) tended to have higher plant-derived C compared to

Table 2
Initial properties of the labeled plant leaf residues used in the study. Shown are means with standard deviations in parenthesis (n=20). Means within the same column followed by different letters are significantly different from each other ($p < 0.05$).

Residue type	C (%)	C:N ratio	$\delta^{13}C$ (‰)
Corn	45.8 (2.2) [a]	11.8 (0.2) [a]	857.4 (168) [a]
Switchgrass	45.8 (2.2) [a]	26.0 (4.0) [b]	576.8 (193) [b]

Table 1
Properties of the large and small pore soil materials obtained from the soils of chisel-plowed corn-soybean-wheat rotation (CSW) and no-till monoculture switchgrass (SG). Shown are means with standard deviations in parenthesis (n=3). Means within the same column followed by different letters are significantly different from each other ($p < 0.05$).

Vegetation History	Pore size	Sand (%)	Silt (%)	Clay (%)	C (%)	N (%)	C:N ratio
CSW	Large	53.2 (0.2) [a]	37.0 (0.8) [a]	9.9 (0.7) [b]	1.2 (0.04) [a]	0.12 (0.004) [a]	10.4 (0.1) [a]
CSW	Small	37.8 (0.2) [b]	48.0 (0.7) [b]	14.2 (0.9) [a]	1.2 (0.05) [a]	0.11 (0.002) [a]	10.6 (0.6) [a]
SG	Large	55.7 (0.5) [a]	37.6 (0.7) [a]	6.7 (1.2) [c]	1.0 (0.03) [b]	0.12 (0.009) [a]	9.6 (0.1) [b]
SG	Small	34.8 (1.0) [b]	55.6 (0.9) [c]	9.5 (1.6) [b]	1.2 (0.08) [a]	0.09 (0.001) [b]	10.4 (0.3) [a]

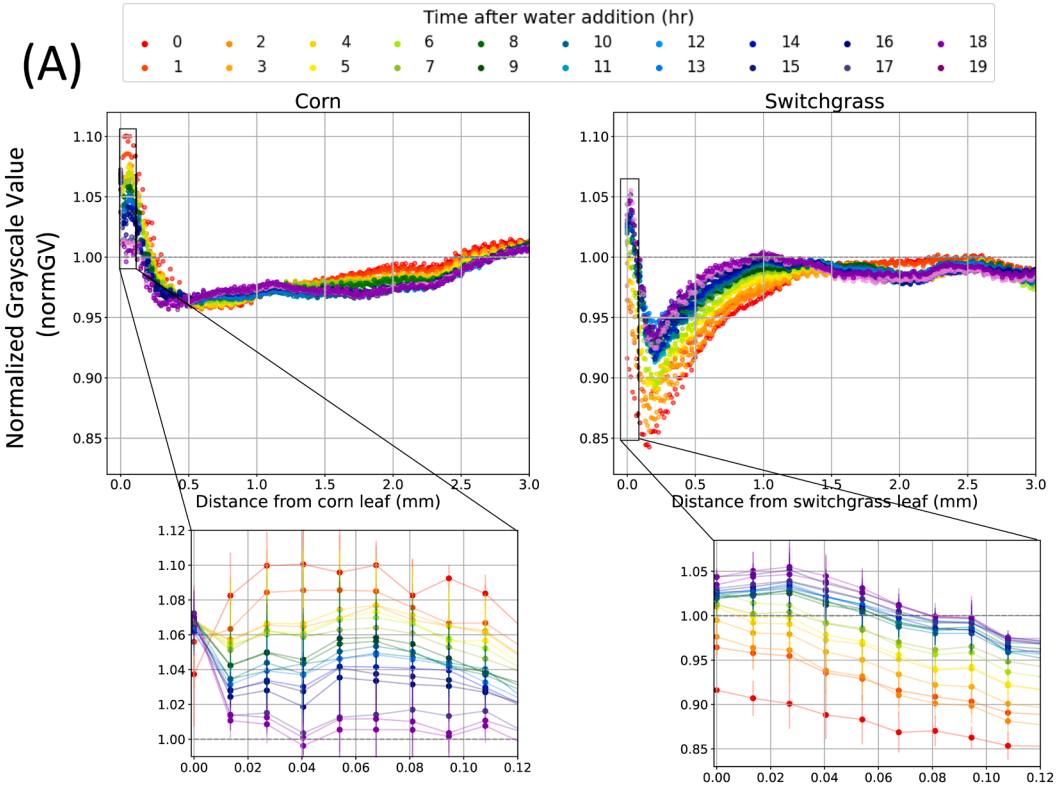

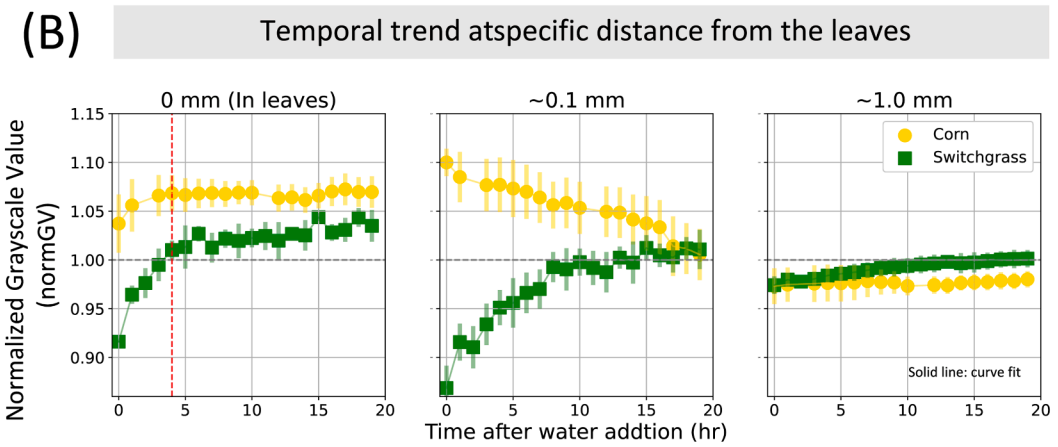

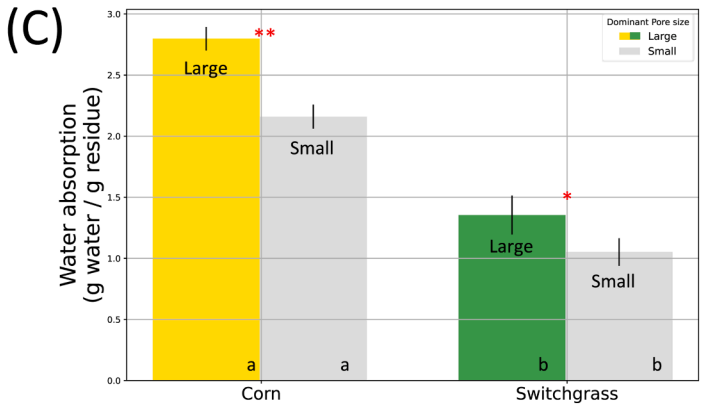

(caption on next page)

Fig. 3. Spatial and temporal patterns of moisture within and around corn and switchgrass leaves incorporated into the large pore soil material. (A) Normalized grayscale values (normGV, representing moisture content) plotted as a function of the distance from corn (left) and switchgrass (right) leaves obtained from nCT images of the large pore microcosms. The colors mark the hourly scans during the incubation ranging from red for the data immediately after the water addition to purple representing the last (19th) hour of the incubation. Gray dotted line marks the mean normGV of the soil in the entire column. (B) Temporal dynamic of normalized grayscale values (moisture content) at distance of 0 mm (left), 0.10 mm (middle), and 1.0 mm (right) from the surface of leaves. Shown are means and standard errors (error bars) from three replicated leaves of each plant. Red dotted line marks the 4 h after the water addition, which corresponds to the water content of the leaves measured during water absorption experiment (presented on C). (C) Moisture content of corn and switchgrass leaves directly measured by the mass increase 4 h after water addition. Asterisks ** and * indicate the significant difference between large and small pore soil materials within each plant with $p < 0.05$ and 0.10, respectively. Different letters mark significant differences in water absorption between corn and switchgrass within each soil pore size ($p < 0.05$). Large pore materials are presented in colors because they are comparable to the samples subjected to nCT and xCT in (A) and (B).

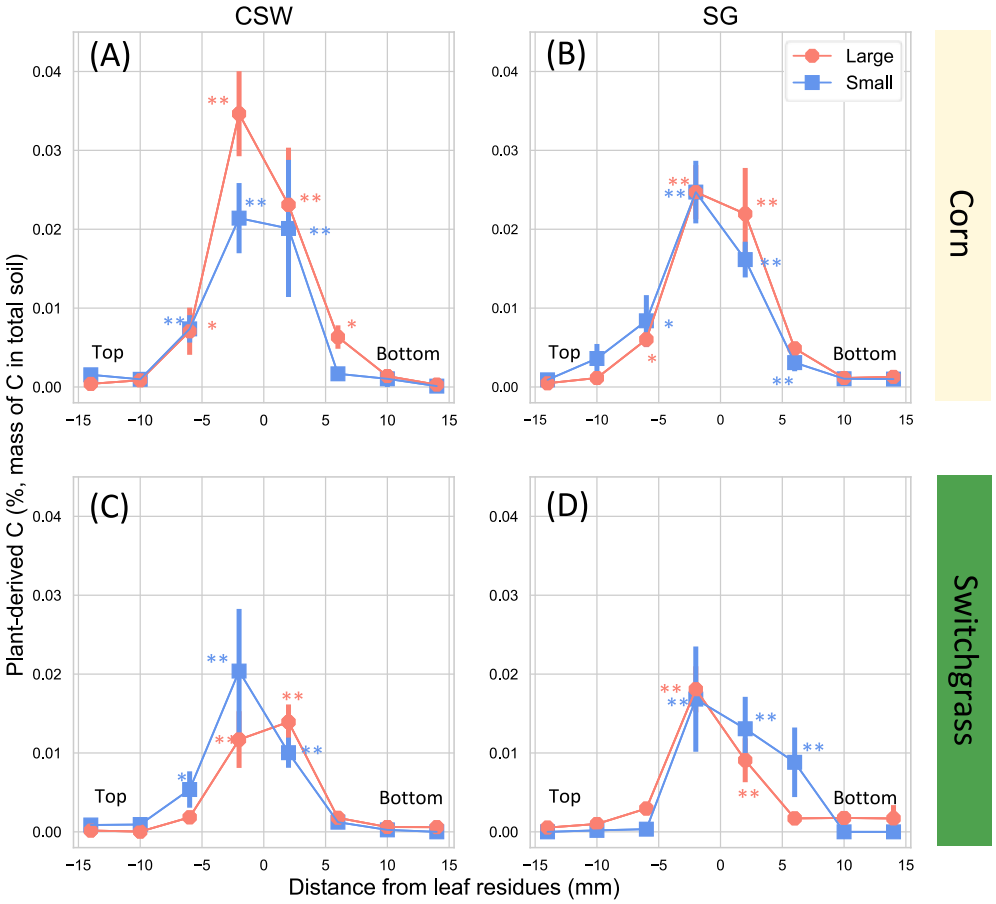

Fig. 4. Plant-derived C (%, mass of plant-derived C in total soil) within the large and small pore materials from corn-soybean-wheat (CSW) and switchgrass (SG) soils as a function of distance from corn (A and B) and switchgrass (C and D) leaves. Error bars present the standard errors of the means. Asterisks ** and * indicate the layers where plant-derived C exceeded zero at significance levels of 0.05 and 0.10, respectively. ANOVA results are provided in Supplementary material (Table S1).

the SG soil ($p < 0.10$), but no statistically significant differences in the plant-derived C were detected between the two pore size materials (Table S1).

3.4. CO_2 emission and priming during plant decomposition

Cumulative CO_2 emission during the 22-day incubation was influenced by vegetation history, pore size, and residue type ($p < 0.01$, Fig. 5A, B, and Table S2). CO_2 emission was 38~82% higher in CSW than in SG soil; it was 21~29% higher in the small pore material than in the large pore one; and $< 10\%$ higher in the microcosms with corn than with switchgrass leaf residue.

Corn residues emitted more plant-derived CO_2 as compared to switchgrass residues ($p < 0.01$, Fig. 5C, D, and Table S2). This trend was more apparent in the large pore material, as indicated by significant interaction between the residue type and pore size ($p < 0.05$) (Table S2). Cumulative Priming effect (PE) was positive, except for the switchgrass leaves incorporated into SG soil, and was 20~66% higher in corn residues compared to switchgrass residues ($p < 0.01$, Fig. 5E, F, and Table S2). In CSW soil, PE triggered by corn residues was more pronounced in the small pore material than in the large pore one ($p < 0.05$).

Temporal dynamic of the plant-derived CO_2 varied depending on the vegetation history ($p < 0.01$) and pore size ($p < 0.05$). But the pore size effect was only apparent in corn residues (interaction between pore size and residue type, $p < 0.10$) (Fig. 6 and Table S3). In contrast to the plant-derived CO_2 emission rate, the fraction of plant-derived CO_2 in the total CO_2 was overall greater in SG than in CSW soil ($p < 0.01$, Table S3). The plant-derived fraction of CO_2 in corn microcosms was higher in the large pore than in the small pore material (Fig. 6A and B), but the pore size effect was not significant in switchgrass microcosms (Fig. 6C and D). Temporal dynamic of CO_2 was clearly affected by the residue type, where corn had the peak of plant-derived CO_2 on day 5–8 decreasing rapidly afterwards, while in switchgrass the peak emissions of plant-derived CO_2 continued till day 15 (Fig. 6).

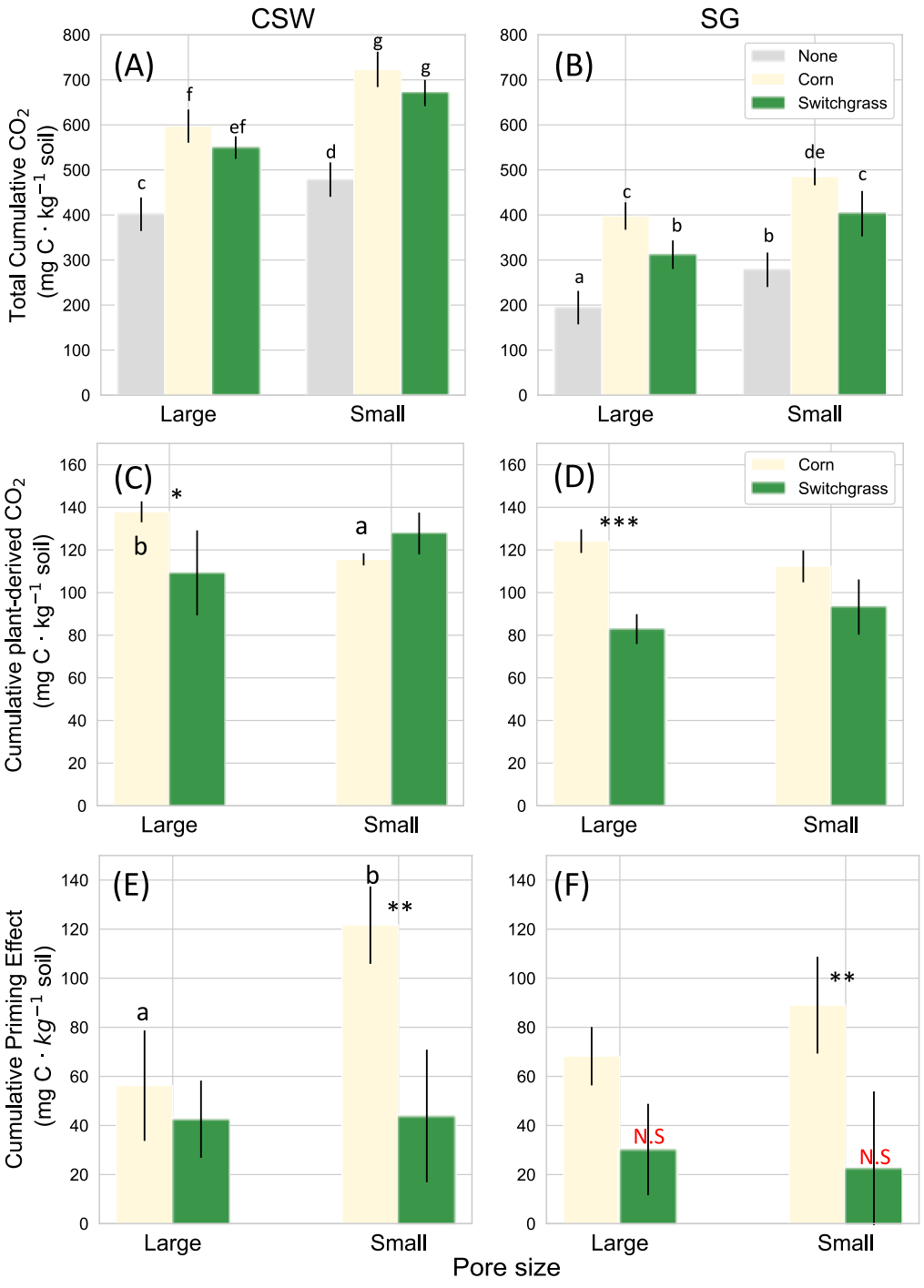

Fig. 5. Cumulative CO_2 emission results during the 22-day incubation: Total cumulative CO_2 emission from (A) CSW and (B) SG soils with and without corn and switchgrass plant residues. In (A) and (B), different letters mark significant differences between treatments (single effects of vegetation history, pore size, and residue type) at $p<0.05$. Cumulative plant-derived CO_2 emission from (C) CSW and (D) SG soils with corn and switchgrass residues. Cumulative priming effect in (E) CSW and (F) SG soil with corn and switchgrass residues. In (C)-(F), the letters mark significant differences between pore sizes in a given vegetation history and residue type. Error bars present the standard errors of the means. Asterisks ***, **, and * indicate significant differences between corn and switchgrass residues at a given vegetation history and pore size with $p < 0.01$, 0.05, and 0.10, respectively. N.S mark the cases when priming effect was not significantly different from 0. ANOVA tables are provided in Supplementary material (Table S2).

3.5. Enzyme activities in detritusphere

β-glucosidase activity in vicinity of the residue increased at the start of the incubation, and the highest activity was achieved in day 8 – 15 (Fig. 7). During that period, the small pore soil material had higher activity than the large pore one except for the switchgrass in CSW soils, and the difference was especially pronounced in the SG soil. β-glucosidase activity was overall higher in SG soil compared to CSW soil ($p < 0.01$, Table S4). β-glucosidase activity around the corn residue in CSW soil (Fig. 7A) was numerically higher when compared to that around switchgrass residue in CSW soil (Fig. 7C), while an opposite trend was observed in SG soil (Fig. 7B and D).

There were no clear temporal trends observed in chitinase activity ($p > 0.10$, Table S4). At the start of the enzyme measurements (day 3 of the incubation), chitinase activity around corn residue in large pore soil was significantly>0 ($p < 0.05$) with a tendency to decrease with time. While on switchgrass residue, it was initially negligible, but with a slightly upward tendency (Fig. 8A and B). In SG soil, higher chitinase activity was observed in large pore materials rather than small pore materials (Fig. 8B and D), whereas there was no significant difference between pore sizes in CSW soil.

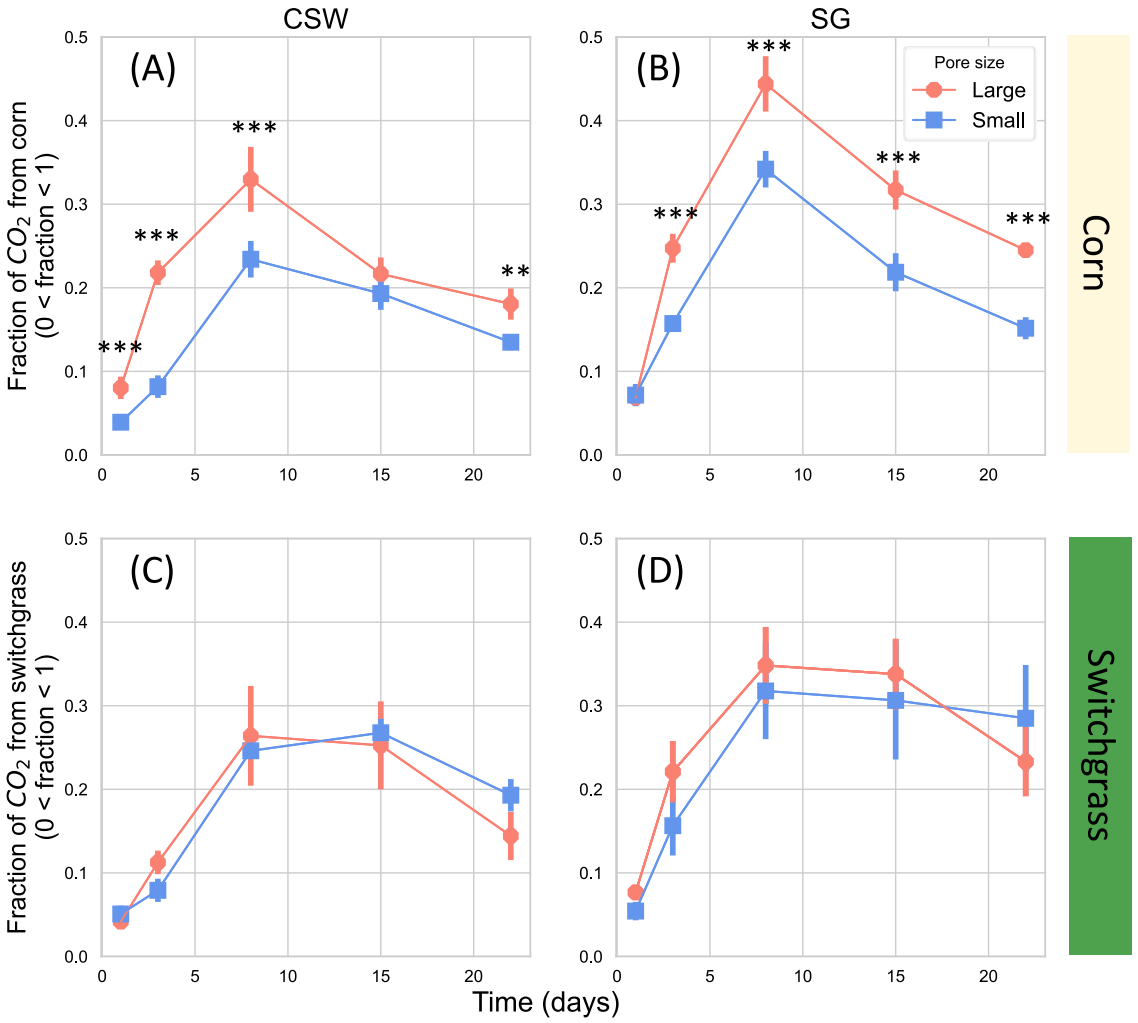

Fig. 6. Fraction of CO_2 derived from corn residue in (A) CSW and (B) SG soil, and fraction of CO_2 derived from switchgrass residue in (C) CSW and (D) SG soil by each day. Black asterisks indicate significant differences between large and small pore materials within each vegetation history, residue type, and day (*** and ** for $p < 0.01$ and 0.05, respectively). Error bars present the standard errors of the means. ANOVA table is provided in Supplementary material (Table S3).

4. Discussion

4.1. Spatiotemporal pattens of water distribution in vicinity of plant residues and their contribution to residue decomposition

As expected, residues incubated within the soil dominated by large pores retained more water than those incubated within the small pore dominated soils (Fig. 3C). Soils with larger pores have lower water retention capacity, which results in higher matric potential gradient in vicinity of plant residue and leads to greater water absorption, as compared to soils with smaller pores (Kravchenko et al., 2017; Kutlu et al., 2018; Kim et al., 2022).

Yet, across both pore size materials, corn leaves retained more water than the switchgrass leaves (Fig. 3C), the observation that emphasizes the importance of inherent plant residue characteristics in defining the magnitude of the sponge effect (Iqbal et al., 2013, Kutlu t al., 2018). Our study for the first time demonstrated that not only the overall absorption of moisture by decomposing plant residue, but also the spatiotemporal dynamics of moisture in the immediate vicinity of the residues can also markedly differ depending on the plant species origin of the residue. Shortly after water addition, moisture (assessed by normGV) in the soil nearby corn leaves was much greater than that in the rest of the soil (Fig. 3B). This observation was consistent with the results of liquid distribution in vicinity of decomposing soybean (*Glycine* max) residues reported by Kim et al. (2020). On the contrary, moisture in the 0.1–1.0 mm soil layer near switchgrass leaves was much lower than that in the rest of the microcosm (Figures 3A and B). The moisture depletion became less severe with incubation time as switchgrass residues, apparently, absorbed some of the surrounding water (Fig. 3B).

The spatiotemporal patterns in moisture distribution formed around the residue then appeared to influence biological activity and residue decomposition. The initial moisture depletion might have delayed the burst of microbial activity and the start of switchgrass residue decomposition as compared to corn. We surmise that lower chitinase activity on switchgrass residues (Fig. 8 and Table S4), lower plant-derived C in vicinity of the switchgrass residues (Fig. 4 and Table S1), and a tendency for lower CO_2 emissions from large pore microcosms with switchgrass residues (Fig. 6 and Table S3) during the first couple of days of incubation, as compared to those of corn, were in part due to the observed initial moisture depletion. The overall higher plant-derived C and CO_2 from microcosms with corn residues than those with switchgrass (Fig. 5 and Table S2) might also be attributed to faster and greater moisture absorption from the corn residues, which stimulates the decomposition (Kim et al., 2022).

While the dynamics of moisture distribution around the residue was studied only in the large pore material, the results from the water absorption experiment (Fig. 3C) suggest that comparable differences between the plant species can be expected in the small pore material as

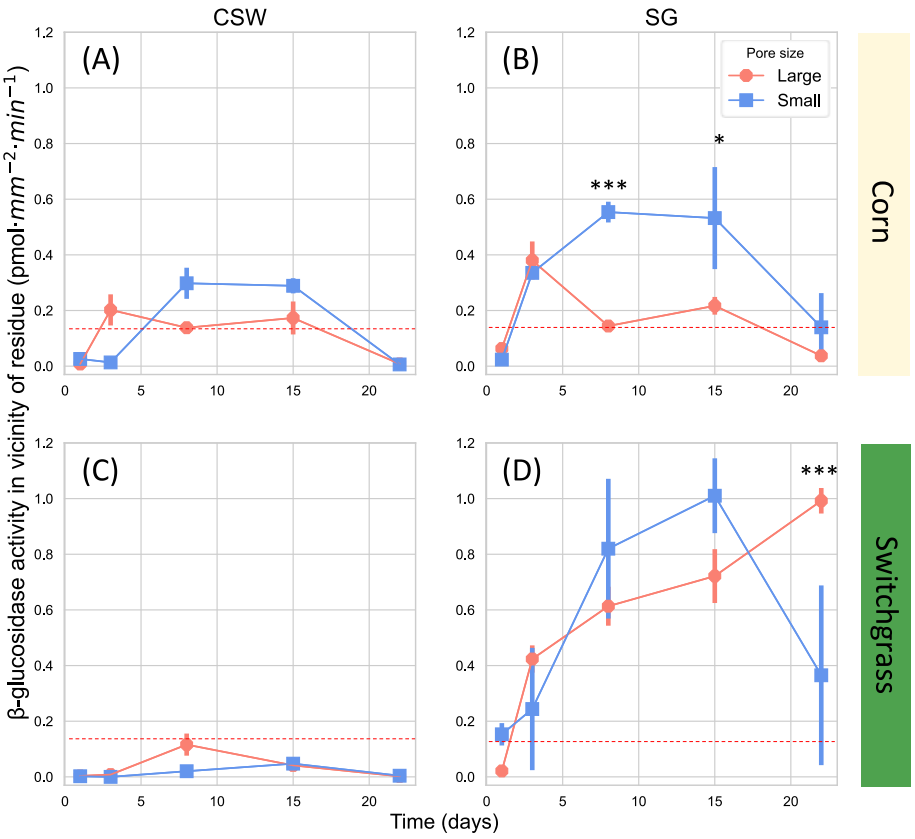

Fig. 7. β-glucosidase activity in vicinity of corn (A and B) and switchgrass (C and D) residues. (A) and (C) are from CSW soil; and (B) and (D) are from SG soil. Error bars present the standard error of means. Asterisks *** and * indicate significant differences between large and small pores in each vegetation history, residue type, and incubation time with $p < 0.01$ and 0.10. The level of chitinase activity is significantly different from zero when the values are above the red dotted lines ($p < 0.05$). ANOVA table was provided in Supplementary material (Table S4).

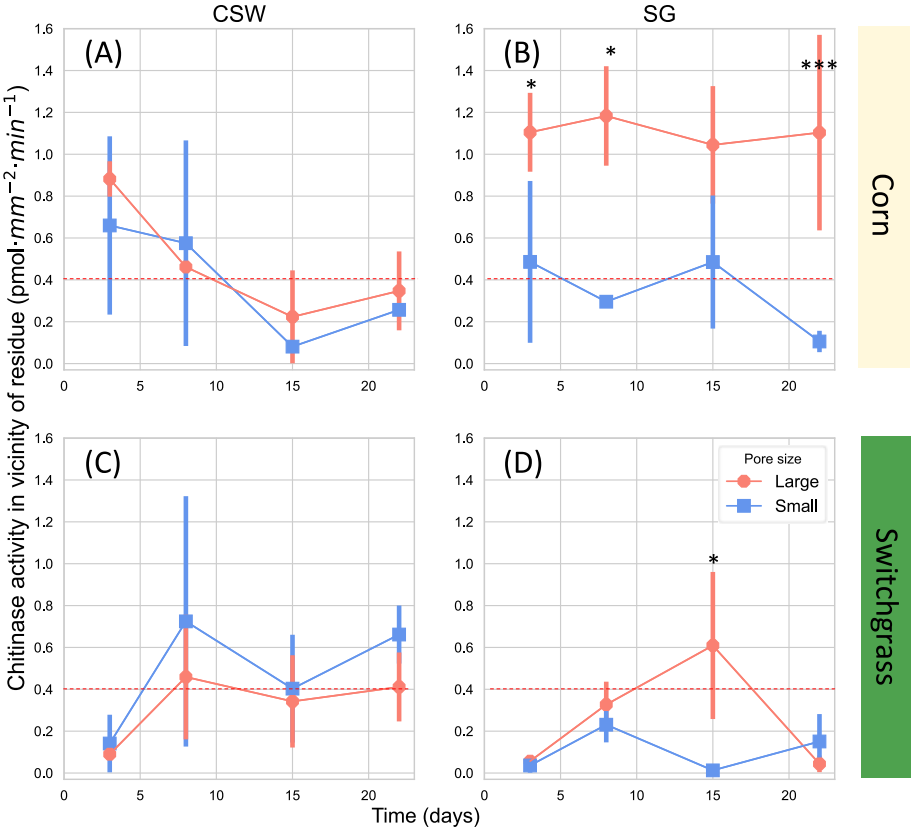

Fig. 8. Chitinase activity in vicinity of corn (A and B) and switchgrass (C and D) residues. (A) and (C) are from CSW soil; and (B) and (D) are from SG soil. Asterisks *** and * indicate significant differences between large and small pores in each vegetation history, residue type, and incubation time with $p < 0.01$ and 0.10. The level of chitinase activity is significantly different from zero when the values are above the red dotted lines ($p < 0.05$). ANOVA table was provided in Supplementary material (Table S4). Error bars present the standard error of means.

well. Indeed, the differences between the quantities of water absorbed by corn and switchgrass leaves after the 4-hr incubation in the two materials were very similar. Specifically, corn leaves absorbed 1.4 g more water per g of residue than the switchgrass leaves in the large pore material and 1.1 g more water per g residue in the small pore material. Still, further studies are needed to explore the role of soil pore characteristics on water distribution in detritusphere.

It should be noted that although the moisture gradients near decomposing residues have been investigated before with xCT (Kim et al., 2020), iodine dopant had to be used in order to obtain quantitative assessments of the distribution, potentially confounding detection of water patterns (Yamaguchi et al., 2010). Here, for the first time the temporal dynamics in distribution of just water in vicinity of plant residues was investigated using nCT.

4.2. Vegetation history, residue type, and pore size effects on soil C dynamics

Plant-derived C from both corn and switchgrass leaves mostly remained within the 4 mm distance from the residues (Fig. 4), which is consistent with previous studies (Gaillard et al., 1999; Gaillard et al., 2003; Vedere et al., 2020). Besides the differences in spatiotemporal patterns of water distribution, differences in chemical characteristics of corn and switchgrass leaves likely added to the observed higher plant-derived C in immediate vicinity of corn than switchgrass leaves in both CSW and SG soils. With their lower C:N ratio (Table 2), corn leaves can be more susceptible to decomposition (Vanlauwe et al., 1996).

Spatiotemporal dynamics of moisture distribution apparently affected the CO_2 emission. In the large pore material, greater decomposition of corn leaves, boosted by higher initial moisture content in their surroundings, led to higher plant-derived C in CO_2 emitted from corn rather than switchgrass leaf microcosms of both CSW and SG soils (Fig. 5C and D). However, in small pore materials, there was no significant difference in plant-derived CO_2 between the plant residues. Instead, greater PE (soil-derived CO_2) was observed from corn when compared to switchgrass across all vegetation history and pore size combinations (Fig. 5E and F). Lower C:N ratio of corn residues (Table 2) can stimulate positive PE by providing more labile C for soil microorganisms (Schmatz et al., 2017). In addition, lower moisture absorption by plant residues in small pore materials (Fig. 3C) suggests possibly longer residence time of the added moisture within the surrounding soil matrix before it was absorbed by the residues, which can stimulate the decomposition of soil organic matter instead of plant residues.

Relatively coarse (4-mm-thick) spatial sectioning of the microcosms in this study did not allow detection of differences in spatial gradients of the plant-derived C (Fig. 4). However, previous work with finer resolution spatial sectioning (Toosi et al., 2017) does suggest that greater diffusion of decomposed substrates into small pore materials might have led to greater PE in the small pore materials.

The peak and total amount of plant-derived CO_2 emission was greater in corn rather than switchgrass (Fig. 6), supporting that the overall quality of residues (e.g., C:N ratio, Table 2) govern the decomposition (Bonanomi et al., 2013; Li et al., 2020). Residue quality can change microbial community structure during the decomposition (Berg and McClaugherty, 2008; Rinkes et al., 2014). Thus, it should be noted that the faster decomposition of corn leaves compared to switchgrass leaves is due to the combined effects of the residue quality and moisture distribution near them.

4.3. Vegetation history, residue type, and pore size effects on enzyme activity

Since the two soils of different vegetation history, CSW and SG, were similar in their intrinsic mineralogical, textural, and chemical characteristics (Table 1), the observed differences in enzyme activities, e.g., much higher β-glucosidase activity in SG than in CSW soil (Fig. 7 and Table S4), most likely originated from the differences in microbial activity and microbial community composition generated by multiple years of contrasting management. Perennial cropping systems are known for their greater microbial community richness and higher microbial biomass as compared to annual systems (Cattaneo et al., 2014; Liang et al., 2012). This was indeed the case for the studied experimental site, where SG soil had greater bacterial and fungal biomasses than the soil of a corn-based system (Jesus et al., 2016).

In SG soil, β-glucosidase activity was higher on the switchgrass than on corn residues, while corn residues induced higher β-glucosidase activity than the switchgrass ones in CSW soil (Fig. 7). In other words, the soil's β-glucosidase activity was higher when the origin of the residue matched the plant species grown in that soil for extended periods of time. This finding is consistent with the home-field advantage (HFA) theory (Gholz et al., 2000), which explains rapid decomposition of plant residues when placed in the soil of the same vegetation history. According to the HFA, local decomposers adapt to the characteristics of plant litter and optimize utilization of available plant litter resources (Gholz et al., 2000; Ayres et al., 2009). Although we did not see corresponding trends in decomposition rates (Fig. 4, Fig. 5C and D), it seems likely that the long-term optimization of CSW and SG microbial communities to their respective corn and switchgrass C sources is what lead to greater -glucosidase production when that familiar source of C was added to the soil (Strickland et al., 2009). It should be noted that no such trend was observed in terms of chitinase activities (Fig. 8). It is inconsistent to the previous report that the HFA for wood decomposition is more related to fungal communities (Purahong et al., 2019), which are primary producers of chitinase (Miller et al., 1998; De Boer et al., 1999; Yanai and Toyota, 2005). In contrast, our results suggested more dominant role of bacteria on HFA, as bacteria serve as primary producers of β-glucosidase (Lupwayi et al., 2018; Zhang et al., 2014). Decomposition of residues with lower C:N ratio, i.e., leaf materials, is contributed more by bacteria rather than fungi (Kathiresan et al., 2011; Grosso et al., 2016), thus the native bacterial community may have significantly contribted to the HFA in this study.

The pore size had an opposite effect on β-glucosidase and chitinase activities. There was an overall higher β-glucosidase activity in the small pore materials during 8 – 15 days of the incubation (Fig. 7), while chitinase activity was higher in the large pore material during the same period in the SG soil (Fig. 8B and D, Table S4). Since higher β-glucosidase activity is often associated with bacterial biomass and activity (Lupwayi et al., 2018; Zhang et al., 2014), higher β-glucosidase activity in small pore materials suggests more active bacterial communities there, flourishing within its relatively small pores and undeterred by the absence of large pores (Schlüter et al., 2018). In contrast, primary producers of chitinase are known to be fungi (Miller et al., 1998; De Boer et al., 1999; Yanai and Toyota, 2005). Fungi prefer larger pores and coarse textured soils, which tend to have larger pores (Kögel-Knabner et al., 2008; Chenu and Cosentino, 2011; Witzgall et al., 2021), similarly to the large pore materials of this study. Thus, high chitinase activity in the large pore materials can be attributed to higher fungal activities. Our results suggest that contrasting soil pore architecture can stimulate activities of different enzymes through the selection of dominant enzyme producers. Further work will be needed to experimentally test this hypothesis.

The initial (at 3 day) chitinase activity in the large pore materials was relatively high on corn residues (Fig. 8A and B) while almost zero on the switchgrass residues (Fig. 8C and D). The observed chitinase activity is not likely to be derived from the soil, because the chitinase activity of the switchgrass in the same soil on day 3 (original soil chitinase activity + newly produced chitinase activity due to corn residue) is almost 0. Thus, the observation suggests that the initial microenvironmental conditions near corn residues incorporated into the large pore soil material were more favorable to chitinase production than that near switchgrass residues. Faster and greater absorption of water by corn residues (Fig. 3) likely led to higher chitinase production and activity

when compared to switchgrass residues. While previous studies suggested that moisture micro-environments can be important controllers of decomposition dynamics (Kravchenko et al., 2017; Toosi et al., 2017; Kim et al., 2021), our results specifically showed that the microscale moisture patterns during initial stages of decomposition play an important role in decomposition dynamics by regulating chitinase activity.

5. Conclusion

This study explored the spatiotemporal dynamics of moisture redistribution near decomposing plant residues using combined xCT and nCT imaging methods. The results suggested, for the first time, that the initial spatial patterns in moisture distribution around the residue within the detritusphere and their subsequent temporal modifications might play an important role in driving microbial activity there, hence influencing CO_2 emission and residue decomposition. This finding emphasizes the importance of detritusphere microenvironments in predicting decomposition dynamics under various soil and plant characteristic settings.

Our study shows that the decomposition dynamics of plant residues is not only a simple function of residue chemistry, but rather a combined effect of the vegetation history, in part through its effect on microbial community composition, the plant residue chemical and likely physical characteristics, and the soil pore structure in the detritusphere. Together, they create temporally dynamic micro-environmental conditions influencing decomposition. We also demonstrate that while the enzymes mediate the decomposition dynamics, temporal trends of individual enzymes and their role in decomposition may differ depending on the soil history and pore structure.

Declaration of Competing Interest

The authors declare that they have no known competing financial interests or personal relationships that could have appeared to influence the work reported in this paper.

Data availability

Data will be made available on request.

Acknowledgements

Authors are indebted to Dr. Andrey Guber for advising on and guiding zymography data collection. Support for this research was provided by the Great Lakes Bioenergy Research Center, U.S. Department of Energy, Office of Science, Office of Biological and Environmental Research (Award DE - SC0018409), by the National Science Foundation Long-term Ecological Research Program (DEB 1832042) at the Kellogg Biological Station, and by Michigan State University AgBioResearch. This work is based on experiments performed at the Swiss spallation neutron source SINQ, Paul Scherrer Institute, Villigen, Switzerland.

Appendix A. Supplementary data

Supplementary data to this article can be found online at https://doi.org/10.1016/j.geoderma.2023.116625.

References

Allison, S.D., Vitousek, P.M., 2004. Extracellular enzyme activities and carbon chemistry as drivers of tropical plant litter decomposition. Biotropica 36 (3), 285–296.
Arcand, M.M., Helgason, B.L., Lemke, R.L., 2016. Microbial crop residue decomposition dynamics in organic and conventionally managed soils. Appl. Soil Ecol. 107, 347–359.
Ayres, E., Steltzer, H., Berg, S., Wall, D.H., 2009. Soil biota accelerate decomposition in high-elevation forests by specializing in the breakdown of litter produced by the plant species above them. J. Ecol. 97, 901–912.
Berg, B., McClaugherty, C., 2008. Plant litter: decomposition, humus formation, carbon sequestration. Springer.
Bogovic, J.A., Hanslovsky, P., Wong, A., Saalfeld, S., 2016. Robust registration of calcium images by learned contrast synthesis, 2016 IEEE 13th International Symposium on Biomedical Imaging (ISBI). IEEE 1123–1126.
Bonanomi, G., Incerti, G., Giannino, F., Mingo, A., Lanzotti, V., Mazzoleni, S., 2013. Litter quality assessed by solid state 13C NMR spectroscopy predicts decay rate better than C/N and Lignin/N ratios. Soil Biol. Biochem. 56, 40–48.
Burns, R.G., DeForest, J.L., Marxsen, J., Sinsabaugh, R.L., Stromberger, M.E., Wallenstein, M.D., Weintraub, M.N., Zoppini, A., 2013. Soil enzymes in a changing environment: current knowledge and future directions. Soil Biol. Biochem. 58, 216–234.
Cattaneo, F., Di Gennaro, P., Barbanti, L., Giovannini, C., Labra, M., Moreno, B., Benitez, E., Marzadori, C., 2014. Perennial energy cropping systems affect soil enzyme activities and bacterial community structure in a South European agricultural area. Appl. Soil Ecol. 84, 213–222.
Chenu, C., Cosentino, D., 2011. Microbial regulation of soil structural dynamics. In: Ritz, K., Young, I. (Eds.), The Architecture and Biology of Soils: Life in Inner Space. CABI, UK, pp. 37–70.
Cotrufo, M.F., Ranalli, M.G., Haddix, M.L., Six, J., Lugato, E., 2019. Soil carbon storage informed by particulate and mineral-associated organic matter. Nat. Geosci. 12 (12), 989–994.
Culman, S.W., DuPont, S.T., Glover, J.D., Buckley, D.H., Fick, G.W., Ferris, H., Crews, T. E., 2010. Long-term impacts of high-input annual cropping and unfertilized perennial grass production on soil properties and belowground food webs in Kansas, USA. Agr Ecosyst Environ 137 (1-2), 13–24.
De Boer, W., Gerards, S., Klein Gunnewiek, P.J.A., Modderman, R., 1999. Response of the chitinolytic microbial community to chitin amendments of dune soils. Biol. Fertil. Soils 29 (2), 170–177.
Gaillard, V., Chenu, C., Recous, S., Richard, G., 1999. Carbon, nitrogen and microbial gradients induced by plant residues decomposing in soil. Eur. J. Soil Sci. 50, 567–578.
Gaillard, V., Chenu, C., Recous, S., 2003. Carbon mineralisation in soil adjacent to plant residues of contrasting biochemical quality. Soil Biol. Biochem. 35 (1), 93–99.
Geisseler, D., Horwath, W.R., Scow, K.M., 2011. Soil moisture and plant residue addition interact in their effect on extracellular enzyme activity. Pedobiologia 54 (2), 71–78.
Georgiou, K., Jackson, R.B., Vindušková, O., Abramoff, R.Z., Ahlström, A., Feng, W., Harden, J.W., Pellegrini, A.F.A., Polley, H.W., Soong, J.L., Riley, W.J., Torn, M.S., 2022. Global stocks and capacity of mineral-associated soil organic carbon. Nat. Commun. 13 (1).
Gholz, H.L., Wedin, D.A., Smitherman, S.M., Harmon, M.E., Parton, W.J., 2000. Long-term dynamics of pine and hardwood litter in contrasting environments: toward a global model of decomposition. Glob. Chang. Biol. 6, 751–765.
Grandy, A.S., Robertson, G.P., 2007. Land-use intensity effects on soil organic carbon accumulation rates and mechanisms. Ecosystems 10 (1), 59–74.
Grosso, F., Bååth, E., De Nicola, F., 2016. Bacterial and fungal growth on different plant litter in Mediterranean soils: effects of C/N ratio and soil pH. Appl. Soil Ecol. 108, 1–7.
Guber, A., Blagodatskaya, E., Juyal, A., Razavi, B.S., Kuzyakov, Y., Kravchenko, A., 2021. Time-lapse approach: correcting deficiencies of 2D soil zymography. Soil Biol. Biochem. 108225.
Guber, A.K., Kravchenko, A.N., Razavi, B.S., Blagodatskaya, E., Kuzyakov, Y., 2019. Calibration of 2-D soil zymography for correct analysis of enzyme distribution. Eur. J. Soil Sci. 70 (4), 715–726.
Hayat, F., Zarebanadkouki, M., Ahmed, M.A., Buecherl, T., Carminati, A., 2020. Quantification of hydraulic redistribution in maize roots using neutron radiography. Vadose Zone J. 19, e20084.
Hoang, D.T.T., Pausch, J., Razavi, B.S., Kuzyakova, I., Banfield, C.C., Kuzyakov, Y., 2016. Hotspots of microbial activity induced by earthworm burrows, old root channels, and their combination in subsoil. Biol. Fertil. Soils 52 (8), 1105–1119.
Hunt, J.R., Celestina, C., Kirkegaard, J.A., 2020. The realities of climate change, conservation agriculture and soil carbon sequestration. Glob. Chang. Biol. 26 (6), 3188–3189.
Iqbal, A., Beaugrand, J., Garnier, P., Recous, S., 2013. Tissue density determines the water storage characteristics of crop residues. Plant and Soil 367 (1-2), 285–299.
Jesus, E.d.C., Liang, C., Quensen, J.F., Susilawati, E., Jackson, R.D., Balser, T.C., Tiedje, J.M., 2016. Influence of corn, switchgrass, and prairie cropping systems on soil microbial communities in the upper Midwest of the United States. GCB Bioenergy 8 (2), 481–494.
Jiang, C., Yu, W., Ma, Q., Xu, Y., Zou, H., 2017. Alleviating global warming potential by soil carbon sequestration: A multi-level straw incorporation experiment from a maize cropping system in Northeast China. Soil Tillage Res. 170, 77–84.
Kaestner, A.P., Hartmann, S., Kühne, G., Frei, G., Grünzweig, C., Josic, L., Schmid, F., Lehmann, E.H., 2011. The ICON beamline–A facility for cold neutron imaging at SINQ. Nucl. Instrum. Methods Phys. Res., Sect. A 659 (1), 387–393.
Kaestner, A., Hovind, J., Boillat, P., Muehlebach, C., Carminati, C., Zarebanadkouki, M., Lehmann, E.H., 2017. Bimodal imaging at ICON using neutrons and X-rays. Phys. Procedia 88, 314–321.
Kasanke, C.P., Zhao, Q., Bell, S., Thompson, A.M., Hofmockel, K.S., 2021. Can switchgrass increase carbon accrual in marginal soils? The importance of site selection. GCB Bioenergy 13 (2), 320–335.

Kathiresan, K., Saravanakumar, K., Anburaj, R., Gomathi, V., Abirami, G., Sahu, S.K., Anandhan, S., 2011. Microbial enzyme activity in decomposing leaves of mangroves. Int. J. Adv. Biotechnol. Res. 2, 382–389.
Kim, K., Guber, A., Rivers, M., Kravchenko, A., 2020. Contribution of decomposing plant roots to N2O emissions by water absorption. Geoderma 375, 114506.
Kim, K., Kutlu, T., Kravchenko, A., Guber, A., 2021. Dynamics of N2O in vicinity of plant residues: a microsensor approach. Plant and Soil 462 (1-2), 331–347.
Kim, K., Gil, J., Ostrom, N.E., Gandhi, H., Oerther, M.S., Kuzyakov, Y., Guber, A.K., Kravchenko, A.N., 2022. Soil pore architecture and rhizosphere legacy define N2O production in root detritusphere. Soil Biol. Biochem. 166, 108565.
Köbke, S., Senbayram, M., Pfeiffer, B., Nacke, H., Dittert, K., 2018. Post-harvest N2O and CO2 emissions related to plant residue incorporation of oilseed rape and barley straw depend on soil NO3-content. Soil Tillage Res. 179, 105–113.
Kögel-Knabner, I., Guggenberger, G., Kleber, M., Kandeler, E., Kalbitz, K., Scheu, S., Eusterhues, K., Leinweber, P., 2008. Organo-mineral associations in temperate soils: Integrating biology, mineralogy, and organic matter chemistry. J. Plant Nutr. Soil Sci. 171 (1), 61–82.
Kravchenko, A., Fry, J., Guber, A., 2018. Water absorption capacity of soil-incorporated plant leaves can affect N2O emissions and soil inorganic N concentrations. Soil Biol. Biochem. 121, 113–119.
Kravchenko, A.N., Toosi, E.R., Guber, A.K., Ostrom, N.E., Yu, J., Azeem, K., Rivers, M.L., Robertson, G.P., 2017. Hotspots of soil N2O emission enhanced through water absorption by plant residue. Nat. Geosci. 10 (7), 496–500.
Kutlu, T., Guber, A.K., Rivers, M.L., Kravchenko, A.N., 2018. Moisture absorption by plant residue in soil. Geoderma 316, 47–55.
Kuzyakov, Y., 2010. Priming effects: interactions between living and dead organic matter. Soil Biol. Biochem. 42 (9), 1363–1371.
Kuzyakov, Y., Friedel, J.K., Stahr, K., 2000. Review of mechanisms and quantification of priming effects. Soil Biol. Biochem. 32 (11-12), 1485–1498.
Lehmann, P., Wyss, P., Flisch, A., Lehmann, E., Vontobel, P., Krafczyk, M., Kaestner, A., Beckmann, F., Gygi, A., Flühler, H., 2006. Tomographical imaging and mathematical description of porous media used for the prediction of fluid distribution. Vadose Zone J. 5 (1), 80–97.
Li, H., Van den Bulcke, J., Kibleur, P., Mendoza, O., De Neve, S., Sleutel, S., 2022. Soil textural control on moisture distribution at the microscale and its effect on added particulate organic matter mineralization. Soil Biol. Biochem. 172, 108777.
Li, Q., Zhang, M., Geng, Q., Jin, C., Zhu, J., Ruan, H., Xu, X., 2020. The roles of initial litter traits in regulating litter decomposition: a "common plot" experiment in a subtropical evergreen broadleaf forest. Plant and Soil 452 (1-2), 207–216.
Liang, C., Jesus, E.d.C., Duncan, D.S., Jackson, R.D., Tiedje, J.M., Balser, T.C., 2012. Soil microbial communities under model biofuel cropping systems in southern Wisconsin, USA: Impact of crop species and soil properties. Appl. Soil Ecol. 54, 24–31.
Liu, M., Chen, X., Chen, S., Li, H., Hu, F., 2011. Resource, biological community and soil functional stability dynamics at the soil–litter interface. Acta Ecol. Sin. 31 (6), 347–352.
Liu, C., Lu, M., Cui, J., Li, B.o., Fang, C., 2014. Effects of straw carbon input on carbon dynamics in agricultural soils: a meta-analysis. Glob. Chang. Biol. 20 (5), 1366–1381.
Lupwayi, N.Z., Kanashiro, D.A., Eastman, A.H., Hao, X., 2018. Soil phospholipid fatty acid biomarkers and β-glucosidase activities after long-term manure and fertilizer N applications. Soil Sci. Soc. Am. J. 82 (2), 343–353.
Marschner, P., Marhan, S., Kandeler, E., 2012. Microscale distribution and function of soil microorganisms in the interface between rhizosphere and detritusphere. Soil Biol. Biochem. 49, 174–183.
McGowan, A.R., Nicoloso, R.S., Diop, H.E., Roozeboom, K.L., Rice, C.W., 2019. Soil organic carbon, aggregation, and microbial community structure in annual and perennial biofuel crops. Agron. J. 111 (1), 128–142.
Miller, M., Palojärvi, A., Rangger, A., Reeslev, M., Kjøller, A., 1998. The use of fluorogenic substrates to measure fungal presence and activity in soil. Appl. Environ. Microbiol. 64 (2), 613–617.
Minasny, B., Malone, B.P., McBratney, A.B., Angers, D.A., Arrouays, D., Chambers, A., Chaplot, V., Chen, Z.-S., Cheng, K., Das, B.S., Field, D.J., Gimona, A., Hedley, C.B., Hong, S.Y., Mandal, B., Marchant, B.P., Martin, M., McConkey, B.G., Mulder, V.L., O'Rourke, S., Richer-de-Forges, A.C., Odeh, I., Padarian, J., Paustian, K., Pan, G., Poggio, L., Savin, I., Stolbovoy, V., Stockmann, U., Sulaeman, Y., Tsui, C.-C., Vågen, T.-G., van Wesemael, B., Winowiecki, L., 2017. Soil carbon 4 per mille. Geoderma 292, 59–86.
Moradi, A.B., Carminati, A., Vetterlein, D., Vontobel, P., Lehmann, E., Weller, U., Hopmans, J.W., Vogel, H.J., Oswald, S.E., 2011. Three-dimensional visualization and quantification of water content in the rhizosphere. New Phytol. 192, 653–663.
Poll, C., Ingwersen, J., Stemmer, M., Gerzabek, M., Kandeler, E., 2006. Mechanisms of solute transport affect small-scale abundance and function of soil microorganisms in the detritusphere. Eur. J. Soil Sci. 57, 583–595.
Poll, C., Marhan, S., Ingwersen, J., Kandeler, E., 2008. Dynamics of litter carbon turnover and microbial abundance in a rye detritusphere. Soil Biol. Biochem. 40 (6), 1306–1321.
Purahong, W., Kahl, T., Krüger, D., Buscot, F., Hoppe, B., 2019. Home-field advantage in wood decomposition is mainly mediated by fungal community shifts at "home" versus "away". Microb. Ecol. 78 (3), 725–736.
Razavi, B.S., Zhang, X., Bilyera, N., Guber, A., Zarebanadkouki, M., 2019. Soil zymography: Simple and reliable? Review of current knowledge and optimization of the method. Rhizosphere 11, 100161.
Rinkes, Z.L., DeForest, J.L., Grandy, A.S., Moorhead, D.L., Weintraub, M.N., 2014. Interactions between leaf litter quality, particle size, and microbial community during the earliest stage of decay. Biogeochemistry 117 (1), 153–168.
Robertson, G.P., Hamilton, S.K., 2015. Long-term ecological research at the Kellogg Biological Station LTER site. Long-term research on the path to sustainability, The ecology of agricultural landscapes, pp. 1–32.
Sanaullah, M., Razavi, B.S., Blagodatskaya, E., Kuzyakov, Y., 2016. Spatial distribution and catalytic mechanisms of b-glucosidase activity at the rootsoil interface. Biol. Fertil. Soils 52, 505–514.
Schindelin, J., Arganda-Carreras, I., Frise, E., Kaynig, V., Longair, M., Pietzsch, T., Preibisch, S., Rueden, C., Saalfeld, S., Schmid, B., Tinevez, J.-Y., White, D.J., Hartenstein, V., Eliceiri, K., Tomancak, P., Cardona, A., 2012. Fiji: an open-source platform for biological-image analysis. Nat. Methods 9 (7), 676–682.
Schlüter, S., Eickhorst, T., Mueller, C.W., 2018. Correlative imaging reveals holistic view of soil microenvironments. Environ. Sci. Tech. 53 (2), 829–837.
Schlüter, S., Leuther, F., Albrecht, L., Hoeschen, C., Kilian, R., Surey, R., Mikutta, R., Kaiser, K., Mueller, C.W., Vogel, H.-J., 2022. Microscale carbon distribution around pores and particulate organic matter varies with soil moisture regime. Nat. Commun. 13, 1–14.
Schmatz, R., Recous, S., Aita, C., Tahir, M.M., Schu, A.L., Chaves, B., Giacomini, S.J., 2017. Crop residue quality and soil type influence the priming effect but not the fate of crop residue C. Plant and Soil 414 (1-2), 229–245.
Seyfried, G.S., Dalling, J.W., Yang, W.H., 2021. Mycorrhizal type effects on leaf litter decomposition depend on litter quality and environmental context. Biogeochemistry 155 (1), 21–38.
Shahbaz, M., Kuzyakov, Y., Heitkamp, F., 2017a. Decrease of soil organic matter stabilization with increasing inputs: mechanisms and controls. Geoderma 304, 76–82.
Shahbaz, M., Kuzyakov, Y., Sanaullah, M., Heitkamp, F., Zelenev, V., Kumar, A., Blagodatskaya, E., 2017b. Microbial decomposition of soil organic matter is mediated by quality and quantity of crop residues: mechanisms and thresholds. Biol. Fertil. Soils 53 (3), 287–301.
Shahbaz, M., Kumar, A., Kuzyakov, Y., Börjesson, G., Blagodatskaya, E., 2018. Priming effects induced by glucose and decaying plant residues on SOM decomposition: a three-source 13C/14C partitioning study. Soil Biol. Biochem. 121, 138–146.
Sinsabaugh, R.L., Moorhead, D.L., 1994. Resource allocation to extracellular enzyme production: a model for nitrogen and phosphorus control of litter decomposition. Soil Biol. Biochem. 26 (10), 1305–1311.
Sinsabaugh, R.L., Lauber, C.L., Weintraub, M.N., Ahmed, B., Allison, S.D., Crenshaw, C., Contosta, A.R., Cusack, D., Frey, S., Gallo, M.E., Gartner, T.B., Hobbie, S.E., Holland, K., Keeler, B.L., Powers, J.S., Stursova, M., Takacs-Vesbach, C., Waldrop, M. P., Wallenstein, M.D., Zak, D.R., Zeglin, L.H., 2008. Stoichiometry of soil enzyme activity at global scale. Ecol. Lett. 11 (11), 1252–1264.
Stewart, C.E., Follett, R.F., Pruessner, E.G., Varvel, G.E., Vogel, K.P., Mitchell, R.B., 2016. N fertilizer and harvest impacts on bioenergy crop contributions to SOC. GCB Bioenergy 8, 1201–1211.
Strickland, M.S., Osburn, E., Lauber, C., Fierer, N., Bradford, M.A., 2009. Litter quality is in the eye of the beholder: initial decomposition rates as a function of inoculum characteristics. Funct. Ecol. 23, 627–636.
Tengattini, A., Lenoir, N., Andò, E., Viggiani, G., 2021. Neutron imaging for geomechanics: A review. Geomech. Energy Environ. 27, 100206.
Thangarajan, R., Bolan, N.S., Tian, G., Naidu, R., Kunhikrishnan, A., 2013. Role of organic amendment application on greenhouse gas emission from soil. Sci. Total Environ. 465, 72–96.
Toosi, E., Kravchenko, A., Guber, A., Rivers, M., 2017. Pore characteristics regulate priming and fate of carbon from plant residue. Soil Biol. Biochem. 113, 219–230.
Tötzke, C., Kardjilov, N., Manke, I., Oswald, S.E., 2017. Capturing 3D water flow in rooted soil by ultra-fast neutron tomography. Sci. Rep. 7, 1–9.
Vanlauwe, B., Nwoke, O.C., Sanginga, N., Merckx, R., 1996. Impact of residue quality on the C and N mineralization of leaf and root residues of three agroforestry species. Plant and Soil 183 (2), 221–231.
Vedere, C., Vieublé Gonod, L., Pouteau, V., Girardin, C., Chenu, C., 2020. Spatial and temporal evolution of detritusphere hotspots at different soil moistures. Soil Biol. Biochem. 150, 107975.
Veres, Z., Kotroczó, Z., Fekete, I., Tóth, J.A., Lajtha, K., Townsend, K., Tóthmérész, B., 2015. Soil extracellular enzyme activities are sensitive indicators of detrital inputs and carbon availability. Appl. Soil Ecol. 92, 18–23.
Witzgall, K., Vidal, A., Schubert, D.I., Höschen, C., Schweizer, S.A., Buegger, F., Pouteau, V., Chenu, C., Mueller, C.W., 2021. Particulate organic matter as a functional soil component for persistent soil organic carbon. Nat. Commun. 12, 1–10.
Yamaguchi, N., Nakano, M., Takamatsu, R., Tanida, H., 2010. Inorganic iodine incorporation into soil organic matter: evidence from iodine K-edge X-ray absorption near-edge structure. J. Environ. Radioact. 101 (6), 451–457.
Yanai, Y., Toyota, K., 2005. Effects of soil freeze-thaw cycles on microbial biomass and organic matter decomposition, nitrification and denitrification potential of soils, Proc. Int. Symp. of JSPS Core to Core Program between Hokkaido University and Martin Luther University Symptom of Environmental Change in Siberian Permafrost Region, Halle-Wittenberg, November 29–30.
Zarebanadkouki, M., Carminati, A., Kaestner, A., Mannes, D., Morgano, M., Peetermans, S., Lehmann, E., Trtik, P., 2015. On-the-fly neutron tomography of water transport into lupine roots. Phys. Procedia 69, 292–298.
Zhang, B., Li, Y., Ren, T., Tian, Z., Wang, G., He, X., Tian, C., 2014. Short-term effect of tillage and crop rotation on microbial community structure and enzyme activities of a clay loam soil. Biol. Fertil. Soils 50 (7), 1077–1085.